



## Parameters affecting reaction rate and conversion of TiO<sub>2</sub> chlorination in a fluidized bed reactor: Experimental and modeling approach

Hossein BORDBAR, Hossein ABEDINI, Ali Akbar YOUSEFI

Iran Polymer and Petrochemical Institute, P. O. Box 14965-115, Tehran, Iran

Received 5 September 2017; accepted 9 January 2018

**Abstract:** Pilot scale chlorination of TiO<sub>2</sub> was carried out with CO as reducing agent. The experimental analysis and modeling of chlorination process of TiO<sub>2</sub> in the presence of CO and Cl<sub>2</sub> in a semi-continuous fluidized bed reactor were aimed. Chlorination process was continuously monitored by measuring the amount of produced TiCl<sub>4</sub> with time. The effects of different operating parameters including chlorination temperature, feedstock particle size and size distribution, amount of feedstock and Cl<sub>2</sub> and CO flow rates on the conversion were systematically investigated. A gradual increase in chlorination temperature led to monotonous increase of conversion rate. Conversion decreased with increased particle size of feedstock. An increase in loaded feedstock led to a decrease in reaction conversion. A model was proposed to predict conversion, particle size distribution and mole fraction of components in gas phase as reaction proceeds. A good agreement between conversions predicted by the model and experimental data under various operating conditions was observed.

**Key words:** chlorination; TiCl<sub>4</sub>; modeling; particle size distribution; conversion

### 1 Introduction

Titanium (Ti) is a metal with the properties of extreme stiffness, lightweight, high resistance against corrosion, low electrical and thermal conductivity, which make it a useful element for widespread applications [1–3]. Almost 95% of titanium is used for production of white TiO<sub>2</sub> pigment [4]. Titanium tetrachloride (TiCl<sub>4</sub>) is an intermediate which is used for production of TiO<sub>2</sub> pigment and titanium sponge [5–8].

Rutile (TiO<sub>2</sub>) and ilmenite (FeO·TiO<sub>2</sub>) are the two principal ores of titanium. Owing to its high titanium content and low levels of impurities, natural rutile has been used as preferred feedstock for the production of titanium dioxide pigment. The principle method in titanium ores treatment is concentration via conventional mineral beneficiation techniques. These methods include Kroll process, sulphate process and chloride process [9–13]. The chloride process is the prevalent process as it generates superior pigment with considerably fewer wastes. Commercial TiCl<sub>4</sub> is produced via fluidized-bed chlorination of rutile or titanium feedstock at 1000–1050 °C in the presence of carbon as reducing agent. The chlorination of

titaniferous ores/slugs is performed by chlorine gas. Fluidized beds provide uniform temperature distributions, low pressure drops, and high heat/mass transfer rates in these processes [14–16].

BERGHOLM [17] studied the chlorination of titania feedstock with carbon and CO and found that the presence of carbon significantly improved the reaction rate. DUNN [18] investigated the chlorination of rutile with carbon and carbon monoxide and reported that small amounts of CO do not affect the reaction rate significantly. However, large additions tend to have a sharp negative effect on reaction kinetics [18]. The effect becomes more serious as carbon particle size decreases and the authors suspected that the CO absorbs onto the carbon surface which in turn prevents the other reagents from reaching the surface. BARIN and SCHULER [19] studied the solid carbon impact on the TiO<sub>2</sub> chlorination in the presence of Cl<sub>2</sub> and CO–CO<sub>2</sub>–Cl<sub>2</sub> gas mixtures. These researchers used discs of rutile and graphite. The rate of chlorination of TiO<sub>2</sub> was observed to be 40 to 50 times faster with TiO<sub>2</sub>–C contact than that without carbon. The acceleration of the chlorination was attributed to the kinetic effect of solid carbon. In the case of impact of solid carbon, it is demonstrated that Cl<sub>2</sub> is chemisorbed at active sites on the carbon surface and

forms C–Cl complexes which, subsequently dissociated and desorbed into the gas phase above 673 K [19].

Studies made about the  $\text{Cl}_2$ –Ni and  $\text{Cl}_2$ –Ti reactions in the presence of solid carbon also showed that activated chlorine species are generated on the carbon surface [19]. These species which are in the form of Cl atoms or Cl-containing radicals or activated  $\text{Cl}_2$  molecules accelerate the chlorination of the metals under investigation [19]. DEN HOED and NELL [20] pointed out that the degree of chlorination increased with increasing carbon content, but decreased at 15% carbon. YOUN and PARK [21] developed a model for fluidized bed chlorination of rutile with coke for production of titanium tetrachloride. SOHN et al [22] investigated the fluidized bed chlorination of natural rutile in  $\text{CO}$ – $\text{Cl}_2$  mixtures. A rate equation was determined in the temperature range of 950–1150 °C. RHEE and SOHN [23] studied the chlorination of ilmenite with  $\text{CO}$  and proposed that the iron in ilmenite reacted with  $\text{Cl}_2$  first and the liberated  $\text{O}_2$  is removed by carbon monoxide. They claimed that the reaction proceeds rapidly at first but then slows down. SOHN and ZHOU [24,25] studied the chlorination kinetics of titania slag with chlorine gas and petroleum coke. A rate equation was established incorporating the effects of temperature, chlorination partial pressure and initial particle size. MOODLEY et al [26,27] chlorinated two titania slags, rutile and synthetic rutile with petroleum coke and  $\text{CO}$  in a small bubbling fluidized bed reactor. Chlorination rate was the highest at 1000 °C; rutile chlorination significantly increased as temperature was increased from 800 to 1000 °C. At 1000 °C, synthetic rutile had the highest chlorination conversion. NIU et al [28] investigated the thermodynamics and kinetics of Kenya natural rutile carbo-chlorination in a fluidized-bed. The thermodynamic calculations of  $\text{TiO}_2$ – $\text{C}$ – $\text{Cl}_2$  system showed the stable presence of titanium tetrachloride and carbon monoxide when C was excess in the solid phase. The appropriate reaction conditions were as follows: reaction temperature of 950 °C, reaction time of 40 min, carbon content of 30% in rutile, natural rutile particle size of 96  $\mu\text{m}$ , petroleum coke size of 150  $\mu\text{m}$ , and chlorine flow of 0.036  $\text{m}^3/\text{h}$  [28]. XIONG et al [29] investigated the effects of carbon/slag molar ratio, chloride amount and temperature on equilibrium molar ratio of  $\text{CO}$  to  $\text{CO}_2$  for off-gas produced by carbochlorination of titanium slag by thermodynamic calculation of equilibrium components of off-gas. Recently, numerous research works have focused on the selective chlorination process to achieve high purity rutile feedstocks [30–36]. WANG and YUAN [37] studied the reductive degree and rate of Bama ilmenite concentrate at different temperatures ranging from 850 to 1400 °C. Due to the presence of some impurities the degree of ilmenite reduction was

decreased. They reported that the rate-controlling steps became different at different temperatures. XIONG et al [38] investigated the purification of crude titanium tetrachloride ( $\text{TiCl}_4$ ) through removing vanadium impurities.  $\text{VOCl}_3$  was converted to insoluble  $\text{VOCl}_2$  by reducing  $\text{TiCl}_4$  to  $\text{TiCl}_3$  through the reaction of Al powder with  $\text{TiCl}_4$  in the presence of white mineral oil. YUAN et al [39] used a multistage series combined fluidized bed reactor assembly to prepare  $\text{TiCl}_4$  in a pilot scale. The combined fluidized bed reactor showed proper anti-agglomeration ability because of  $\text{MgCl}_2$  and  $\text{CaCl}_2$  accumulation on the surface of unreacted slag which left the reactor [39].

A laboratory study on the chlorination of anatase was carried out with  $\text{CO}$  as reducing agent. This work is coupled with the modeling of chlorination process of  $\text{TiO}_2$  in the presence of  $\text{CO}$  and  $\text{Cl}_2$  in a semi-continuous fluidized bed reactor. The proposed model can predict the conversion, the particle size distribution of  $\text{TiO}_2$  particles and mole fraction of gases in the reactor. The conversion rate predicted by the modeling results was compared with the experimental data obtained under various operating conditions. The effect of different operating parameters on the conversion was investigated. The conversion, and the amount of  $\text{TiCl}_4$  produced during the chlorination process was continuously monitored as a function of time which provides an accurate estimation of chlorination process and chlorination product. This continuous monitoring of the  $\text{TiCl}_4$  production adopted in this work has higher accuracy for determination of amount of  $\text{TiCl}_4$  produced and distinguishes the present work from other works in the literature. The novelty of present work is that the conversion of chlorination was continuously monitored with reaction time by measuring amount of  $\text{TiCl}_4$  in a graduated cylinder obtained during the reaction.

## 2 Experimental

### 2.1 Materials

The  $\text{TiO}_2$  (anatase) used in this work was an EC E171 grade provided by EINECS, India. The typical specifications of the  $\text{TiO}_2$  (anatase) as determined by X-ray fluorescence (XRF) analysis are listed in Table 1. The size distribution of anatase particles is given in Table 2. The  $\text{CO}$  was used as reducing agent. The chlorine, carbon monoxide, and nitrogen gases were all supplied by Roham Gas Co., Ltd., Iran.

**Table 1** Typical specifications of  $\text{TiO}_2$  (anatase) used in this work (mass fraction, %)

$\text{TiO}_2$	$\text{K}_2\text{O}$	$\text{MgO}$	$\text{Fe}_2\text{O}_3$	$\text{Al}_2\text{O}_3$	$\text{CaO}$	$\text{Nb}_2\text{O}_5$
99.58	0.23	0.07	0.01	0.05	0.03	0.03

**Table 2** Size distribution of anatase

Anatase particle size/ $\mu\text{m}$	Mass fraction/%
850	1.7
420	30.7
250	21.3
180	10
150	19.3
75	14.7
<75	0.6

## 2.2 Apparatus and procedures

The chlorination of anatase was carried out in a fluidized-bed reactor which consisted of a gas inlet system, a quartz reactor and a product gas cooling system. A schematic diagram of the experimental apparatus used in this work is shown in Fig. 1. The height of quartz reactor was 120 cm with internal diameters of 25 mm and 50 mm for lower and upper sections of the reactor, respectively. The internal diameter of upper section of reactor was adjusted to reduce the flow velocity and minimize the leaving particles from the reactor.

An electric resistance furnace surrounds the quartz tube to ensure the required reaction temperature. In order to uniformly distribute the fluidizing gas, a porous disk was placed in the lower part of the quartz tube. The particulate feedstock containing titanium was poured on the distributor. The gas flow rate was measured using rotameters. Gas mixed, and entered fluidized-bed where they were heated.  $\text{TiO}_2$  feedstock was charged into the

reactor at first, and then the  $\text{N}_2$  in the reactor was driven off by pumping nitrogen gas. After temperature reached the setting point, the nitrogen gas flew into the reactor was gradually decreased and replaced by the chlorine and CO gases. After the holding time elapsed, nitrogen was increased instead chlorine gas to drive residual chlorine gas.

At the end of each test, the system was cooled at a controlled cooling rate so as to prevent any thermal stress and/or shock in the reactor system. The chlorinated slag was removed and weighed when its temperature fell down. The obtained  $\text{TiCl}_4$  was collected in a vessel and by probing its production with time, the reaction rate and the conversion were measured. Then, attempt was made to calibrate the product obtained by weighing the obtained  $\text{TiCl}_4$ .

The final degree of conversion ( $X_f$ ) was calculated by the following equations:

$$X_f = \frac{m_{\text{chlorinated}}}{m_{\text{initial}}} \times 100\% \quad (1)$$

$$m_{\text{chlorinated}} = m_{\text{initial}} - m_{\text{bed}} \quad (2)$$

where  $m_{\text{chlorinated}}$  is the chlorinated mass (g),  $m_{\text{initial}}$  is the mass of initial feedstock (g), and  $m_{\text{bed}}$  is the mass of feedstock remaining in the bed (g). The ultimate conversion at the end of chlorination process was determined by above equations. Then, the conversion rate ( $X$ ) at any time was determined from ultimate conversion ( $X_f$ ) at the end of chlorination process and the amount of  $\text{TiCl}_4$  produced at that time ( $m_{\text{TiCl}_4}$ ) by continuous monitoring.

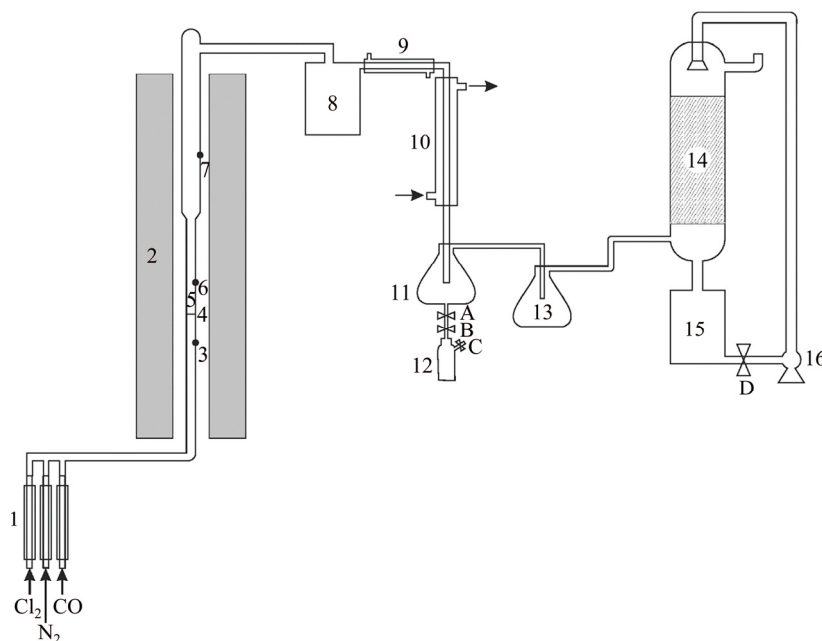


**Fig. 1** Schematic diagram of experimental apparatus used in this work: 1—Rotameters; 2—Furnace; 3—Thermocouple; 4—Gas distributor; 5—Solid reactant; 6, 7—Thermocouples; 8—Cyclone; 9, 10—Cooling tubes; 11—Trap; 12—Graduated cylinders; 13—Trap; 14—NaOH quench tower (NaOH scrubber); 15—NaOH solution reservoir; 16—Pump

The conversion at any time was calculated by the following equation:

$$X = X_f \frac{m_{\text{TiCl}_4}^f}{m_{\text{TiCl}_4}^f} \quad (3)$$

where  $m_{\text{TiCl}_4}^f$  is the mass of  $\text{TiCl}_4$  produced at the end of chlorination process.

The parameters of the experiment set are given in Tables 3–7. The effects of operational parameters such as chlorine gas flow rate (Table 3), amount of feedstock (Table 4), CO gas flow rate (Table 5), feedstock particle size distribution (Table 6) and reaction temperature (Table 7) on the efficiency and productivity of the  $\text{TiCl}_4$  product were studied in this work. Moreover, attempt was made to simulate the chlorination process of titanium containing feedstock by mathematical modeling, and the results were compared with the experimental data obtained from chlorination process.

**Table 3** Effect of chlorine gas flow rate on chlorination process

No.	$m_{\text{TiO}_2}/\text{g}$	Particle size range/ $\mu\text{m}$	$T/^\circ\text{C}$	$v(\text{CO})/(\text{L}\cdot\text{min}^{-1})$	$v(\text{Cl}_2)/(\text{g}\cdot\text{h}^{-1})$	$v(\text{N}_2)/(\text{L}\cdot\text{min}^{-1})$
1	25	180–420	1050	1	50	0.3
2	25	180–420	1050	1	75	0.3
3	25	180–420	1150	1	50	0.3
4	25	180–420	1150	1	75	0.3

**Table 4** Results of amount of feedstock

No.	$m_{\text{TiO}_2}/\text{g}$	Particle size range/ $\mu\text{m}$	$T/^\circ\text{C}$	$v(\text{CO})/(\text{L}\cdot\text{min}^{-1})$	$v(\text{Cl}_2)/(\text{g}\cdot\text{h}^{-1})$	$v(\text{N}_2)/(\text{L}\cdot\text{min}^{-1})$
1	25	180–420	1150	1	75	0.15
2	50	180–420	1150	1	75	0.15

**Table 5** Effects of CO flow rate on chlorination process

No.	$m_{\text{TiO}_2}/\text{g}$	Particle size range/ $\mu\text{m}$	$T/^\circ\text{C}$	$v(\text{CO})/(\text{L}\cdot\text{min}^{-1})$	$v(\text{Cl}_2)/(\text{g}\cdot\text{h}^{-1})$	$v(\text{N}_2)/(\text{L}\cdot\text{min}^{-1})$
1	25	180–420	1150	0.5	75	0.15
2	25	180–420	1150	1	75	0.15

**Table 6** Parameters of chlorination at 1150 °C for different size distributions

No.	$m_{\text{TiO}_2}/\text{g}$	Particle size range/ $\mu\text{m}$	$T/^\circ\text{C}$	$v(\text{CO})/(\text{L}\cdot\text{min}^{-1})$	$v(\text{Cl}_2)/(\text{g}\cdot\text{h}^{-1})$	$v(\text{N}_2)/(\text{L}\cdot\text{min}^{-1})$
1	25	180–420	1150	1	75	0.15
2	25	420–850	1150	1	75	0.15
3	25	<180 $\mu\text{m}$	1150	1	75	0.15

**Table 7** Parameters of chlorination reaction at different temperatures

No.	$m_{\text{TiO}_2}/\text{g}$	Particle size range/ $\mu\text{m}$	$T/^\circ\text{C}$	$v(\text{CO})/(\text{L}\cdot\text{min}^{-1})$	$v(\text{Cl}_2)/(\text{g}\cdot\text{h}^{-1})$	$v(\text{N}_2)/(\text{L}\cdot\text{min}^{-1})$
1	25	180–420	1050	1	75	0.15
2	25	180–420	1150	1	75	0.15

### 2.3 Mathematical modeling of reactor

The mass balance for  $\text{TiO}_2$  consumption is given by the following equation:

$$\frac{dm_{\text{TiO}_2}}{dt} = -R_{\text{TiO}_2} S M_r \quad (4)$$

where  $R_{\text{TiO}_2}$  is the rate of  $\text{TiO}_2$  consumption,  $S$  is the surface area of particles at any time and  $M_r$  is the relative molecular mass of  $\text{TiO}_2$ . The  $R_{\text{TiO}_2}$  and  $S$  parameters are defined as follows:

$$R_{\text{TiO}_2} = k p_{\text{Cl}_2}^n p_{\text{CO}}^m \quad (5)$$

$$k = k_0 \exp[-E/(RT)] \quad (6)$$

$$S = 4\pi \sum_{i=1}^N n_i r_i^2, \quad n_i = \frac{m_{i0}}{\frac{4}{3}(\rho_s \pi r_{i0}^3)} \quad (7)$$

where  $p_{\text{Cl}_2}^n$  and  $p_{\text{CO}}^m$  are the pressures of  $\text{Cl}_2$  and  $\text{CO}$ , respectively;  $\rho_s$  is the density of  $\text{TiO}_2$  particles;  $r_{i0}$  is the particle radius at the instant  $t=0$ ; and  $m_{i0}$  is the mass of particles with radius  $r_{i0}$ .

The change of particles' diameter in each population was determined by

$$\frac{-dr_i}{dt} = \frac{R_{\text{TiO}_2} M_r}{\rho_s} \quad (i=1 \cdots N; \quad m_i = \frac{4}{3} n_i \rho_s \pi r_i^3) \quad (8)$$

where  $r_i$  is the particle radius at time  $t$ , and  $m_i$  is the mass of particles with radius  $r_i$ .

The mass balance of components in gas phase by assuming the reactor as a CSTR reactor can be written as

$$VC \frac{dy_j}{dt} = F_j^f - C y_j Q_g - R_j S \quad (j=\text{CO}, \text{Cl}_2, \text{TiCl}_4, \text{CO}_2) \quad (9)$$

$$R_{\text{CO}} = R_{\text{Cl}_2} = 2R_{\text{TiO}_2} \quad (10)$$

$$R_{\text{TiCl}_4} = -R_{\text{TiO}_2} \quad (11)$$

$$R_{\text{CO}_2} = -2R_{\text{TiO}_2} \quad (12)$$

where  $V$  is the volume of the reaction section in the reactor,  $C$  is the total concentration of gases, and  $y_j$  is the mole fraction of matter  $j$  in the gas phase.

The total volume flow rate is given by

$$Q_g = \frac{\dot{m}_{\text{g,in}} + R_{\text{TiO}_2} S M_r}{\rho_g} \quad (13)$$

where  $\dot{m}_{g,in}$  is the mass flow rate of input gas mixture and  $\rho_g$  is the gas density. The  $\rho_g$  is given by

$$\rho_g = CM_r^{av} \quad (14)$$

where  $M_r^{av}$  stands for the average relative molecular mass of gas phase. The  $C$  and  $M_r^{av}$  parameters are defined as

$$C = p/(RT) \quad (15)$$

$$M_r^{av} = \sum_{j=1}^5 y_j M_{r,j} \quad (16)$$

$$y_{N_2} = 1 - \sum_{j=1}^4 y_j \quad (17)$$

The ordinary differential equations ((4), (8) and (9)) and other algebraic equations ((5)–(7), (10)–(17)) were solved using MATLAB Ode solver in a variable step mode with respect to time, simultaneously.

Assuming the uniform particle size distribution of  $TiO_2$  particles, the following equation was used [22,24,25,40]:

$$1 - (1 - X)^{1/3} = kd^{-1} p_{Cl_2}^n p_{CO}^m \quad (18)$$

The values of  $m$ ,  $n$  and  $E$  were obtained by plotting  $1 - (1 - X)^{1/3}$  versus time and calculation of the slope of plots at the low conversion rates under various operating conditions. The obtained values were as follows:  $n=1.18$ ,  $m=0.65$  and  $E=110.24$  kJ/mol, where  $E$  is the activation energy.

## 3 Results and discussion

### 3.1 Effect of chlorine gas flow rate

The effects of chlorine gas flow rate at two different temperatures on the chlorination process are given in Table 3. At 1050 and 1150 °C, the conversions obtained for chlorine gas flow rates were set at 50 and 75 g/h, respectively.

The effects of flow rate of chlorine on the conversion and reaction rate of anatase feedstock at two

different temperatures are shown in Fig. 2. The data in Fig. 2 further show that at a given chlorination temperature, the conversion in terms of initial slope of conversion vs time tends to increase as the chlorine gas flow rate is increased. Moreover, at a fixed chlorine gas flow rate the data reveal that the conversion enhanced as the chlorination temperature was increased from 1050 to 1150 °C. The increased conversion with an increase in the chlorine gas flow rate can be due to the intensity during the chlorination reaction at higher flow rates. The results also show a good agreement between the experimental data and model results.

The model predictions for variation of particle size distribution at different time for two concentrations of  $Cl_2$  (50 and 75 g/h) are shown in Figs. 3 and 4, respectively. According to Figs. 3 and 4, the smaller particles undergo a faster mass reduction owing to their higher surface area and this trend is more pronounced when the flow rate of  $Cl_2$  is 75 g/h. This finding is consistent with the data reported in Refs. [21,25,28].

### 3.2 Effect of amount of feedstock

The data obtained for chlorination process of  $TiO_2$  feedstock at two levels of initial feedstock with the particle sizes in the range of 180–420  $\mu m$  are displayed in Table 4. These data can provide insight into the effect of feedstock loading on the conversion of anatase ore.

The conversion rate vs time plots for two levels of feedstock (25 and 50 g) obtained at 1150 °C are shown in Fig. 5(a). Figure 5(a) further displays that the conversion rate of 25 g feedstock is significantly higher than that of 50 g feedstock. The large amount of initial feedstock may hinder the efficient mass and heat transfer during the chlorination process, which in turn is manifested by a decrease in the conversion. Moreover, an increase in the anatase feedstock would lead to a decrease in the  $(CO, Cl_2)/TiO_2$  mole ratio which means that a lower amount of CO reductant and  $Cl_2$  are available for chlorination process of anatase feedstock. As a result, the conversion is decreased as the  $(CO, Cl_2)/TiO_2$  mole ratio was

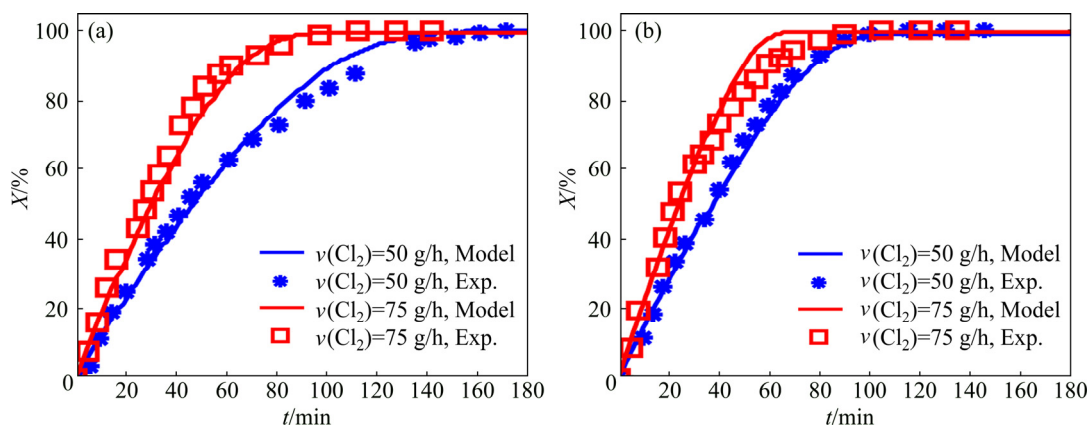
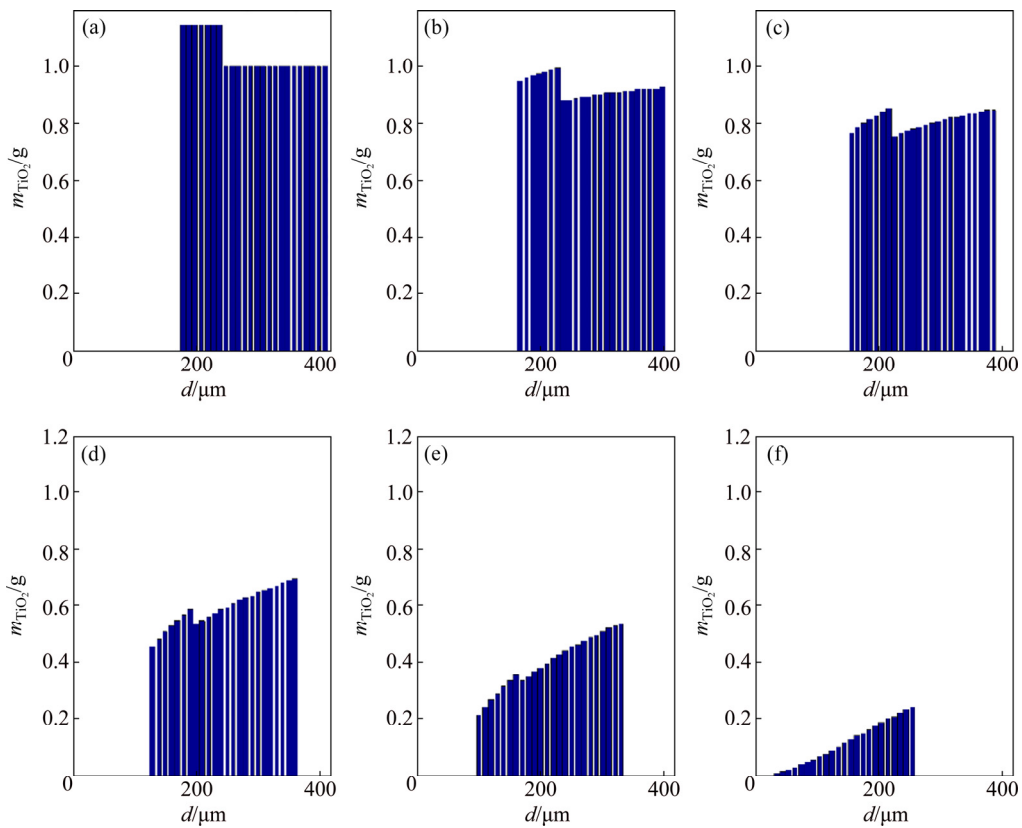
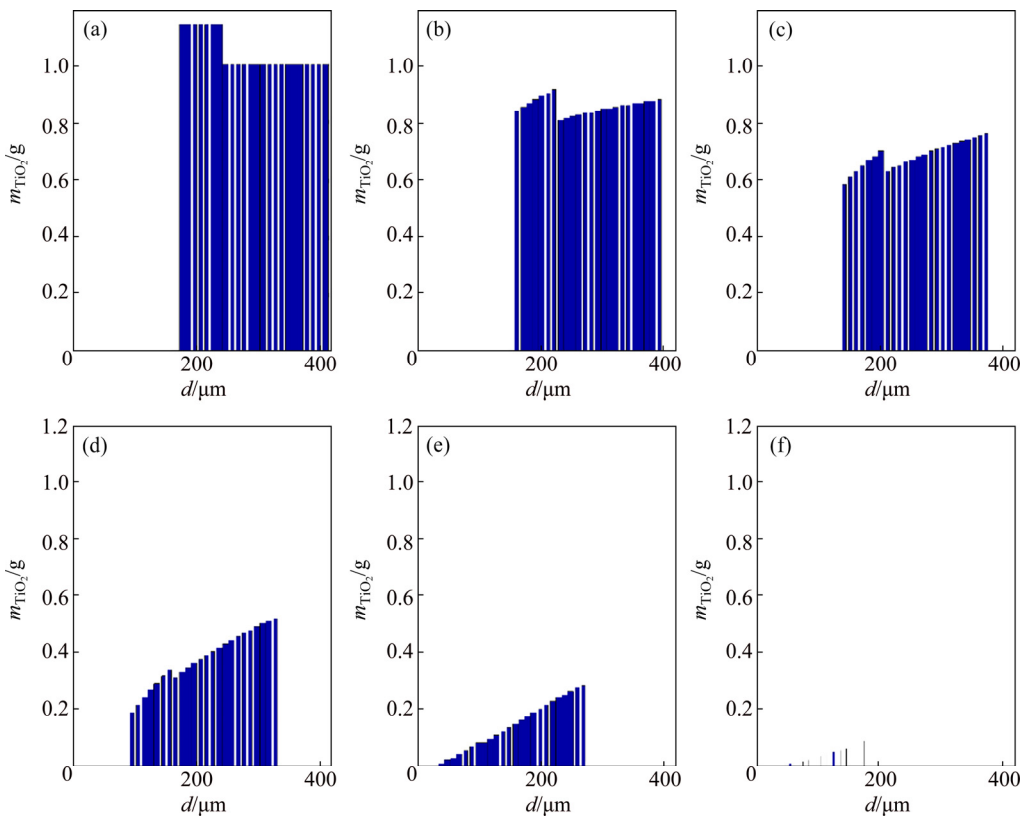


Fig. 2 Effect of flow rate of chlorine on ultimate conversion ( $X$ ) of anatase at different temperatures: (a) 1050 °C; (b) 1150 °C



**Fig. 3** Particle size distribution evolution with time at 1050 °C and Cl<sub>2</sub> flow rate of 50 g/h: (a)  $t=0$  min; (b)  $t=10$  min; (c)  $t=20$  min; (d)  $t=40$  min; (e)  $t=60$  min; (f)  $t=100$  min



**Fig. 4** Particle size distribution evolution with time at 1050 °C and Cl<sub>2</sub> flow rate of 75 g/h: (a)  $t=0$  min; (b)  $t=10$  min; (c)  $t=20$  min; (d)  $t=40$  min; (e)  $t=60$  min; (f)  $t=80$  min

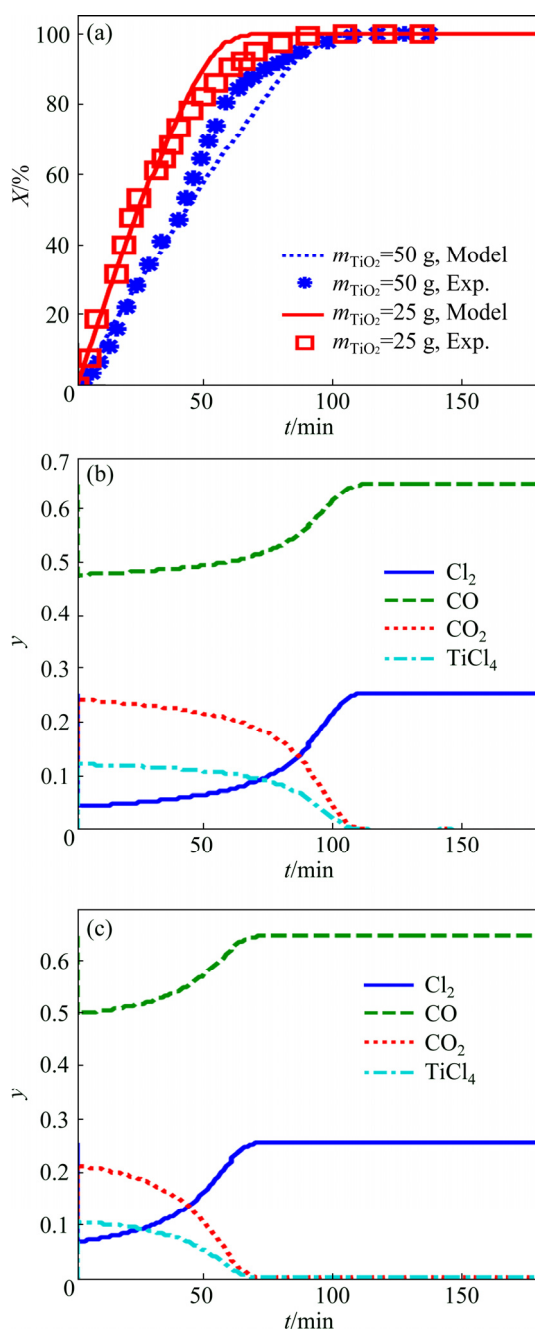


**Fig. 5** Conversion vs time for different feedstock masses  $m_{\text{TiO}_2}$  at 1150 °C (a), mole fraction of reactor outlet gases vs time for  $m_{\text{TiO}_2}=50\text{ g}$  (b) and  $m_{\text{TiO}_2}=25\text{ g}$  (c)

reduced. This decrease in reaction rate and conversion rate is due to a decrease in the  $\text{Cl}_2$  and  $\text{CO}$  gas in reactor as shown in Figs. 5(b) and (c).

Figures 5(b) and (c) show that the concentrations of  $\text{Cl}_2$  and  $\text{CO}$  in the reactor are not constant during the reaction time. Upon consumption of  $\text{TiO}_2$  with time, the concentrations of  $\text{Cl}_2$  and  $\text{CO}$  in the reactor approach to those of inlet values and after complete conversion in Figs. 5(b) and (c), the mole fractions of  $\text{TiCl}_4$  and  $\text{CO}_2$  at the reactor outlet become zero and the mole fractions of  $\text{Cl}_2$  and  $\text{CO}$  turn into the inlet values.

### 3.3 Effect of CO flow rate

The effects of CO flow rate on the conversion of a given anatase sample during the chlorination process for certain operational conditions are given in Table 5.

The effects of CO flow rate on the conversion of  $\text{TiO}_2$  feedstock at 1150 °C are shown in Fig. 6. Regarding the data presented in Fig. 6 the effect of CO flow rate on the conversion of chlorination reaction can be investigated. As seen in Fig. 6, the conversion and reaction rate increase as the CO flow rate increases. Considering the fact that CO serves as reducing agent in the chlorination process, the increase in the CO flow rate promotes the chlorination reaction and is favorable to the kinetics of chlorination process [28].

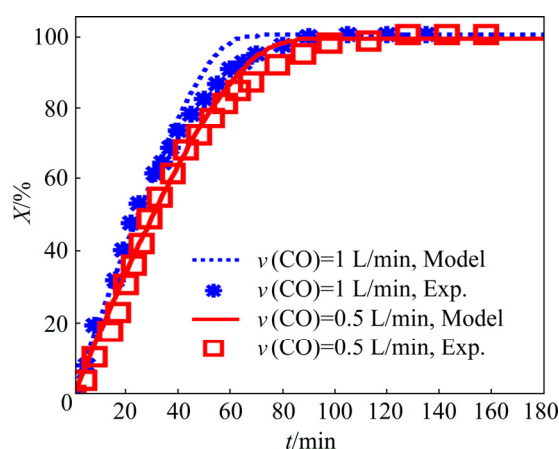


**Fig. 6** Effect of flow rate of CO on conversion of anatase feedstock at 1050 °C

### 3.4 Effect of size distribution at 1150 °C

The results of chlorination process for feedstocks of different particle size distributions at the temperature of 1150 °C are summarized in Table 6.

The conversion vs time plots for different feedstocks obtained at 1150 °C are shown in Fig. 7(a). Figure 7(a) also demonstrates the effect of particle size of anatase on the conversion. As seen, the feedstock with particle sizes less than 180  $\mu\text{m}$  reveals the highest conversion and reaction rate as compared with the other feedstocks. This may be due to the fact that the larger particles have smaller specific surface area (Fig. 7(b)), which adversely affects the kinetic conditions of chlorination reaction [28]. The smaller feedstock particles with greater specific surface area are more favorable for chlorination reaction.

Figures 7(b) and 8 demonstrate that the reduction in contact surface area of particle becomes more intense as the particle size decreased. The data reveal that the smallest particles show the highest drop in surfaces area as a function of reaction time. As mentioned, the surface area of the particles gradually increases as the particle size decreases. The increase in contact surface area is

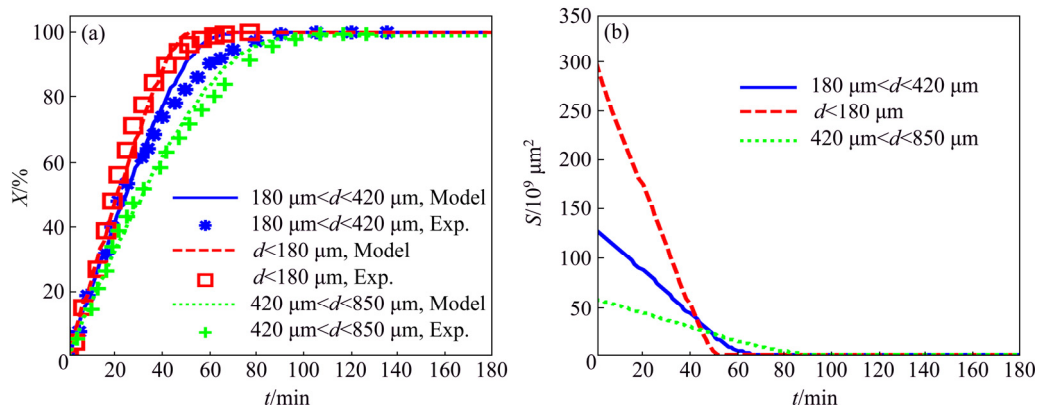


**Fig. 7** Conversion vs time (a) and reaction area vs time (b) for feedstocks of different particle sizes at 1150 °C

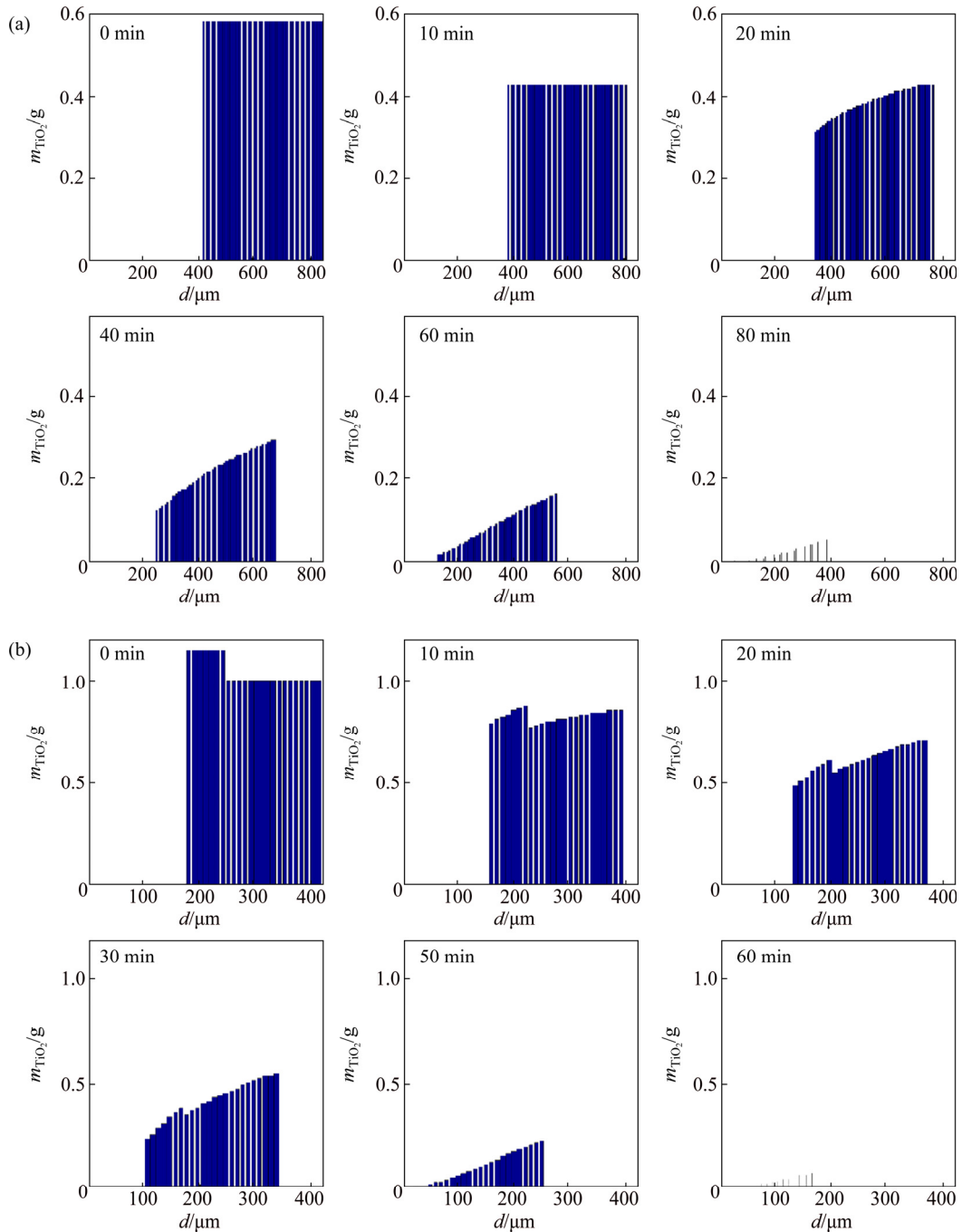


**Fig. 8** Particle size distribution evolution with time at 1050 °C and  $\text{Cl}_2$  flow rate of 75 g/h for feedstocks with different particle sizes: (a) 420–850  $\mu\text{m}$ ; (b) 180–420  $\mu\text{m}$

favorable to greater reaction rate and conversion rate. Consequently, the decrease in contact surface area with time is more significant for smaller particles than that of the larger ones. The above mentioned results are in a good agreement with research works by YOUN and PARK [21], SOHN and ZHOU [25] and NIU et al [28].

### 3.5 Effect of reaction temperature

The results of chlorination process at two operating temperatures (1050 °C and 1150 °C) for feedstock with the particle sizes in the range of 180–420 μm are listed in Table 7.

The conversion vs time plots for feedstock with particle sizes in the range of 180–420 μm obtained at different temperatures are shown in Fig. 9. From Fig. 9, one can see the effect of temperature on the conversion and reaction rate. As seen, the slope of initial stage of conversion vs time curves gradually increases as the chlorination temperature was increased, indicating that the conversion tends to increase with the chlorination temperature. The difference between the experimental conversion data for chlorination at 1050 and 1150 °C (Fig. 9) is insignificant up to 40 min of reaction time; afterwards the difference between the conversions appears. These findings are again confirmed by the results of other researchers [21,22,25–28].

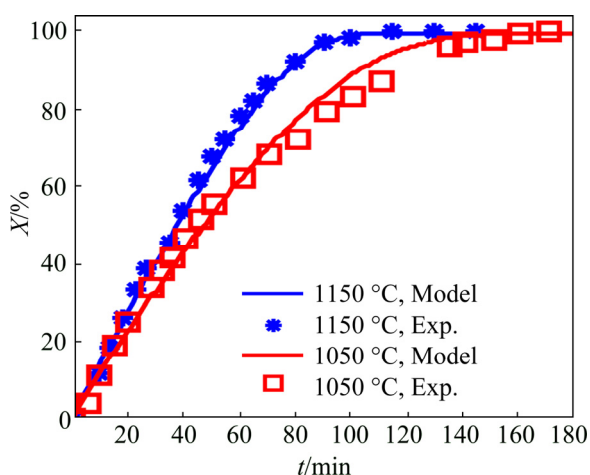


**Fig. 9** Conversion vs time for feedstock with particle size in range of 180–420 μm at two different temperatures

As seen in Fig. 9, the reaction rate and conversion undergo a considerable increase as the temperature was increased. This is because the reaction rate of particles with  $\text{Cl}_2$  and thereby the generation of  $\text{TiCl}_4$  is enhanced at higher temperature. As a result, the rate of contact surface area reduction becomes more intense with increasing temperature. Figure 9 shows that there is a good agreement between the experimental data and

theoretical results.

## 4 Conclusions

1) Chlorination of  $\text{TiO}_2$  was carried out in the presence of CO as reducing agent. The effects of chlorination temperature (1050 and 1150 °C), feedstock particle size and size distribution, amount of feedstock and  $\text{Cl}_2$  and CO flow rates on the conversion and the reaction rate were studied experimentally and theoretically.

2) A new model was developed to predict changes in particle size distribution with time, conversion rate and molar fraction of components in the gas phase as reaction proceeds inside the reactor. The predictions of the proposed model for the conversion rate at different temperatures, various concentrations of CO and  $\text{Cl}_2$ , different amounts of  $\text{TiO}_2$  fed into the reactor and different sizes of feedstock particles were in good agreement with the experimental data.

3) The effects of operating conditions including feedstock particle size and size distribution, amount of feedstock, chlorination temperature, and  $\text{Cl}_2$  and CO flow rates on the conversion were also studied. In case of  $\text{TiO}_2$  (anatase) feedstock with the particles in the range of 180–420 μm, it was found that with gradual increase in chlorination temperature from 1050 to 1150 °C, the conversion rate and reaction rate were monotonically increased.

4) In the case of size and size distribution, the highest reaction rate was obtained for anatase feedstock containing particles smaller than 180 μm. It was observed that an increase in loading of feedstock led to a decrease in conversion rate and reaction rate. Increase in the chlorine gas flow rate at both 1050 and 1150 °C increased the conversion and reaction rate as the chlorine gas flow rate was increased. The conversion rate of anatase was increased as the CO flow rate of chlorination process was increased from 0.5 to 1 L/min.

## References

- [1] KOTHARI N C. Recent developments in processing ilmenite for titanium [J]. International Journal of Mineral Proceedings, 1974, 1: 287–305.
- [2] BUDINSKI K G. Surface engineering for wear resistance [M]. Englewood Cliffs: Prentice Hall, 1988: 420–460.
- [3] KNITTEL D. Titanium and titanium alloys [M]// Encyclopedia of chemical technology. GRAYSON M. 3rd Edition. Hoboken: John Wiley and Sons, 1983: 98–130.
- [4] GAZQUEZ M J, BOLIVAE J P, GARICA-TENORIO R, VACA F. A review of the production cycle of titanium dioxide pigment [J]. Materials Sciences and Applications, 2014, 5: 441–458.

- [5] RUDNICK R L, GAO S. Composition of the continental crust [M]// Treatise of geochemistry, RUDNICK R L. Vol. 3. Amsterdam: Elsevier, 2003.
- [6] GAMBOGI J. Titanium, 2007 minerals yearbook [M]. Washington DC: U.S. Government Printing Office, US Geological Survey, 2009: 195–220.
- [7] STWERTKA A. Guide to the elements [M]. Revised Edition. London: Oxford University Press, 1998: 240–270.
- [8] WILLIAMS V A. WIM 150 Detrital heavy mineral deposit [M]// Geology of the mineral deposits of Australia and Papua new guinea, Monograph 14. HUGHES F E. Australasian: Australasian Institute of Mining and Metallurgy, 1990: 1609–1614.
- [9] WHITEHEAD J. Titanium compounds (Inorganic) [M]// Encyclopedia of chemical technology, 3rd Edition. GRAYSON M. Hoboken: John Wiley and Sons, 1983: 131–176.
- [10] KROLL W. Vergütbare Titanlegierungen [J]. Metallurgical Wirtschaft, 1930, 9: 1043–1045.
- [11] KROLL W. The production of ductile titanium [J]. Transaction of Electrochemical Society, 1940, 78: 35–47.
- [12] KROLL W. Methods for manufacturing titanium and alloys: U.S. Patent 2, 205 [P]. 1940: 854.
- [13] KALE A, BISAKA K. Fluid bed chlorination pilot plant at Mintek [J]. Journal of the Southern African Institute of Mining and Metallurgy, 2011, 111(3): 193–197.
- [14] SAU D C, MOHANTY S, BISWAL K C. Minimum fluidization velocities and maximum bed pressure drops for gas–solid tapered fluidized beds [J]. Chemical Engineering Journal, 2007, 132: 151–157.
- [15] ESCUDERO D, HEINDEL T J. Minimum fluidization velocity in a 3D fluidized bed modified with an acoustic field [J]. Chemical Engineering Journal, 2013, 231: 68–75.
- [16] SHABANIAN J, CHAOUKI J. Effects of temperature, pressure, and interparticle forces on the hydrodynamics of a gas-solid fluidized bed [J]. Chemical Engineering Journal, 2017, 313: 580–590.
- [17] BERGHOLM A. Titanium tetrachloride and iron from ilmenite [J]. Jernkont Ann, 1961, 145: 1–205.
- [18] DUNN W E. High temperature chlorination of titanium dioxide bearing minerals [J]. Transactions AIME, 1960, 218: 6–12.
- [19] BARIN I, SCHULER W. On the kinetics of the chlorination of titanium dioxide in the presence of solid carbon [J]. Metallurgical Transactions B, 1980, 11B: 199–207.
- [20] DEN HOED P, NELL J. The carbochlorination of titaniferous oxides in a small scale fluidised bed [J]. IFSA, 2002, 133–143.
- [21] YOUN I J, PARK K Y. Modeling of fluidized bed chlorination of rutile [J]. Metallurgical Transactions B, 1989, 20B: 959–966.
- [22] SOHN H Y, ZHOU L, CHO K. Intrinsic kinetics and mechanism of rutile chlorination by CO and Cl<sub>2</sub> mixtures [J]. Industrial Engineering Chemistry Research, 1998, 37: 3800–3805.
- [23] RHEE K I, SOHN H Y. The selective chlorination of iron from ilmenite ore by CO–Cl<sub>2</sub> Mixtures: Part 1: Intrinsic kinetics [J]. Metallurgical Transactions, 1990, 21B: 321–329
- [24] SOHN H Y, ZHOU L. The kinetics of carbochlorination of titania slag [J]. Canadian Journal of Chemical Engineering, 1998, 76: 1078–1082.
- [25] SOHN H Y, ZHOU L. The chlorination kinetics of beneficiated ilmenite particles by CO+Cl<sub>2</sub> mixtures [J]. Chemical Engineering Journal, 1999, 72: 37–42
- [26] MOODLEY S. A study of the chlorination behaviour of various titania feedstocks [D]. Johannesburg: University of the Witwatersrand, 2011: 1–154.
- [27] MOODLEY S, KALE A, BESSINGER D, KUCUKKARAGOZ C, ERICH R H. Fluidization behaviour of various titania feedstocks [J]. Journal of Southern African Institute of Mining and Metallurgy, 2012, 112: 467–471.
- [28] NIU L P, NI P Y, ZHANG T A, LV G Z, ZHOU A P, LIANG X, MEN D. Mechanism of fluidized chlorination reaction of Kenya natural rutile ore [J]. Rare Metals, 2014, 33: 485–492.
- [29] XIONG Shao-feng, YUAN Zhang-fu, XU Cong, XI Liang. Composition of off-gas produced by combined fluidized bed chlorination for preparation of TiCl<sub>4</sub> [J]. Transactions of Nonferrous Metals society of china, 2010, 20(1): 128–134.
- [30] BECKER P, GLENK F, KORMANN M, POPOVSKA N, ETZOLD B J M. Chlorination of titanium carbide for the processing of nanoporous carbon: A kinetic study [J]. Chemical Engineering Journal, 2010, 159: 236–241.
- [31] KANG J, OKABE T H. Production of titanium dioxide directly from titanium ore through selective chlorination using titanium tetrachloride [J]. Materials Transactions, 2014, 55: 591–598.
- [32] GUO Y, HE J, JIANG T, LIU S, ZHENG F, WANG S. Preparation of synthetic rutile from titanium slag [C]// 5th International Symposium on High-Temperature Metallurgical Processing. Hoboken, NJ, USA: John Wiley & Sons, Inc., 2014: 531–537.
- [33] YANG K, PENG J, ZHANG L, ZHU H, CHEN G, ZHENG X, TAN X, ZHANG S. Research on microwave roasting of high titanium slag process [C]// 5th International Symposium on High-Temperature Metallurgical Processing. Hoboken, NJ, USA: John Wiley & Sons, Inc., 2014: 579–588.
- [34] MAHARAJH S, MULLER J, ZIETSMAN J H. Value-in-use model for chlorination of titania feedstocks [J]. Journal of the southern African Institute of Mining and Metallurgy, 2015, 115(5): 385–394.
- [35] DMITRIEV A N, PETUKHOV R V, VITKINA G Y, CHESNOKOV Y A, KORNILKOV S V, PELEVIN A E. The reduction processes of the titanium containing iron ores treatment: Defect and diffusion forum [J]. Trans Tech Publications, Switzerland, 2016, 369: 6–11.
- [36] YUAN Z, WANG X, XU C, LI W, KWAIK M. A new process for comprehensive utilization of complex titania ore [J]. Miner Eng, 2006, 19: 975–978.
- [37] WANG Y, YUAN Z. Reductive kinetics of the reaction between a natural ilmenite and carbon [J]. International Journal of Mineral Processing, 2006, 81: 133–140
- [38] XIONG S, YUAN Z, YIN Z, YAN W. Removal of the vanadium impurities from crude TiCl<sub>4</sub> with high content of vanadium using a mixture of Al power and white mineral oil [J]. Hydrometallurgy 2012, 119–120: 16–22.
- [39] YUAN Z, ZHU Y, XI L, XIONG S, XU B. Preparation of TiCl<sub>4</sub> with multistage series combined fluidized bed [J]. Transactions of Nonferrous Metals Society of China, 2013, 23: 283–288.
- [40] MORRIS A J, JENSEN R F. Fluidized-bed chlorination rates of Australian rutile [J]. Metall Trans B, 1976, 7: 89–93.

## 影响流化床反应器中 $\text{TiO}_2$ 氯化反应速率和转化率的参数：实验和模拟方法

Hossein BORDBAR, Hossein ABEDINI, Ali Akbar YOUSEFI

Iran Polymer and Petrochemical Institute, P. O. Box 14965-115, Tehran, Iran

**摘要：**以 CO 为还原剂，进行中试规模的  $\text{TiO}_2$  氯化。在 CO 和  $\text{Cl}_2$  存在的条件下，对半连续流化床反应器中的  $\text{TiO}_2$  氯化过程进行实验分析和模拟。通过测量  $\text{TiCl}_4$  生成量随时间的变化，连续监测氯化过程。系统研究氯化温度、原料粒径和粒度分布、原料量、 $\text{Cl}_2$  和 CO 流速等操作参数对转化率的影响。逐渐升高氯化温度导致转化率单调上升。随着原料粒度的增大，转化率降低，负载量的增加导致反应转化率下降。提出一个预测反应过程中转化率、粒径分布和气相组分摩尔分数的模型。在不同的操作条件下，模型预测的转化率与实验数据吻合良好。

**关键词：**氯化； $\text{TiCl}_4$ ；模拟；粒度分布；转化

(Edited by Xiang-qun LI)